Much more than a toxin: hydrogen cyanide is a volatile modulator of bacterial behaviour

Abhishek Anand[1], Laurent Falquet[1], Eliane Abou-Mansour[1], Floriane L'Haridon[1], Christoph Keel[2] & Laure Weisskopf[1]*

[1]Department of Biology, University of Fribourg, Fribourg, Switzerland

[2]Department of Fundamental Microbiology, University of Lausanne, Lausanne, Switzerland

***Correspondence:**

Prof. Laure Weisskopf

Department of Biology

University of Fribourg

Chemin du musée 10

CH-1700 Fribourg

Switzerland

Tel: +41 26 300 88 11

Email: laure.weisskopf@unifr.ch

Introductory paragraph

Bacteria communicate with each other and with other organisms in a chemical language comprising both diffusible and volatile molecules, and volatiles have recently gained increasing interest as mediators of bacterial interactions[1]. One of the first volatile compounds discovered to play a role in biotic interactions is hydrogen cyanide (HCN)[2], a well-known toxin, which irreversibly binds to the key respiratory enzyme cytochrome C oxidase[3]. The main ecological function of this molecule was so far thought to lie in the inhibition of competing microorganisms[4]. Here we show that HCN is much more than a respiratory toxin and should be considered a major regulator of bacterial behaviour rather than a solely defensive secondary metabolite. Cyanogenesis occurs in both environmental and clinical *Pseudomonas* strains[5,6]. Using cyanide-deficient mutants in two *Pseudomonas* strains, we demonstrate that HCN functions as an intracellular and extracellular volatile signalling molecule, which leads to global transcriptome reprogramming affecting growth, motility, and biofilm formation, as well as the production of other secondary metabolites such as siderophores and phenazines. Our data suggest that bacteria are not only using endogenous HCN to control their own cellular functions, but are also able to remotely influence the behaviour of other bacteria sharing the same environment.

Cyanogenesis occurs in many different types of organisms, including bacteria, plants, animals and even humans[7–9]. In bacteria, most studies have focused on *Pseudomonas* strains, which form HCN by oxidative decarboxylation of glycine[4]. HCN is considered an important virulence factor in both environmental (e.g. *Pseudomonas protegens* CHA0) and clinical (e.g. *Pseudomonas aeruginosa* PAO1) strains[2,10]. The ecological role of HCN emission in bacterial defence against competing organisms is well established and this molecule has been repeatedly pinpointed as a major actor in the arsenal of root-associated *Pseudomonas* with protective effects against plant diseases[11]. An earlier study using comparative genomics to identify the molecular determinants of late blight control by potato-associated *Pseudomonas* highlighted HCN as a likely candidate accounting for the inhibition of the devastating oomycete pathogen *Phytophthora infestans*[12]. However, when we compared the anti-*Phytophthora* effects of cyanogenesis-deficient mutants in two different species of *Pseudomonas* with that of their respective wild types, we noticed only little to no reduction in their antagonistic potential. Moreover, we observed that the mutants had gained additional antimicrobial capacities, e.g. inducing higher inhibition of the pathogen's zoospore germination[13]. This prompted us to quantify the mutants' secretion of siderophores, as these iron-chelators are well-known mediators of antifungal activity[14]. We first grew both strains on King's B medium, which is classically used to detect siderophores in pseudomonads (Figure 1a). Compared to the *Escherichia coli* control, our two model strains *Pseudomonas chlororaphis* R47 and *Pseudomonas putida* R32 secreted siderophores as evidenced by the halo surrounding the colonies. In *P. putida* R32, the HCN-deficient mutant appeared to produce more siderophores than the wild type, while the difference was less clear for R47 in this qualitative plate assay. Since we knew from these two strains' genomes that they both encoded pyoverdine production, we used a fluorospectrometry-based assay[15] to quantify the production dynamics of this particular siderophore as well as the growth of both wild types and mutants in liquid King's B

medium (Figure 1b). No significant growth difference between wild type and mutant was observed in R32, but the production of pyoverdine was increased in the mutant. For R47, a growth advantage was observed for the mutant at the onset of stationary phase, yet the strong increase in pyoverdine production was in no proportion to this moderate growth advantage (Figure 1b). The orange colour of R47 (Figure 1a) originates from the production of phenazines, an important class of antimicrobial compounds, also involved in iron acquisition, redox balance, and many other biological functions in *Pseudomonas* strains[16]. We therefore also quantified the production of phenazine carboxylic acid (PCA), one particular form of phenazines, in both wild type and HCN-deficient mutant strains grown in King's B medium. We analysed this phenotype only in *P. chlororaphis* R47, since phenazine biosynthetic genes are not encoded in the genome of *P. putida* R32. We observed that similarly to pyoverdine, PCA was also produced at a higher concentration (>2.5-fold) by the mutant than by the wild type (Figure 1c). Next to PCA, other phenazines were also produced more abundantly in the absence of HCN production (Figure S1). Taken together, these data indicate that the absence of HCN led to a significantly enhanced production of other secondary metabolites that could fulfil similar ecological functions such as inhibition of microbial competitors.

The ability to move towards a favourable environment and once there, to form a biofilm are relevant features for successful colonization of both plant (e.g. roots) and human (e.g. lung) tissues by pseudomonads[17,18].We therefore wondered whether motility and biofilm formation would also be influenced by the loss of cyanogenesis in our two *Pseudomonas* mutants. Our swimming motility assays on low agar plates revealed that both HCN-deficient mutants were significantly (ca. 2-fold) more motile than the wild types (Figure 1d). In contrast to all previous phenotypes tested, where the mutants performed better than the wild types, biofilm formation was significantly lower for both mutants compared to the wild types (Figure 1e). In addition to

confirming the expected negative relation between a motile and a sessile life style, these data also provided the proof of concept that HCN also stimulated and not only inhibited physiological processes in cyanogenic pseudomonads. Overall, the consistent observation in two different *Pseudomonas* species that the loss of cyanogenesis led to effects as diverse as enhanced siderophore production and reduced biofilm formation, confirmed our hypothesis that HCN is more than a mere respiratory toxin, and likely a global regulator of bacterial physiology and behaviour.

In order to test this hypothesis, we selected *P. chlororaphis* R47 because of its large genome encoding many secondary metabolites[12] and compared the transcriptome of wild type and mutant grown in liquid King's B medium at three different time points (Figure 2a). We chose these time points to cover i) the early log phase, at which we did not expect any change since HCN, as a secondary metabolite, was classically reported to be produced at the end of the exponential growth phase[19], ii) the transition between exponential and stationary phase, at which HCN effects were expected to start taking place, and iii) the later stationary phase, at which we expected changes to be further amplified (Figure 2a). In contrast to our expectation, the transcriptomes of wild type and HCN-deficient mutant already clustered separately at the early log phase (Figure 2b). Looking at the expression of the HCN biosynthetic operon, we observed that it was indeed already expressed at the early exponential phase (Figure S2), and its absence induced the dysregulation of 32 genes belonging to different COG categories already at this time point (Figure 2c and Table S1). Among these, genes involved in signal transduction and lipid transport / metabolism were mainly upregulated in absence of HCN, while genes involved in transcription, amino acid and carbohydrate metabolism, inorganic ion transport and secondary metabolism were mainly downregulated in the mutant. Genes belonging to the energy production and conversion category were also dysregulated, with some

being up- and others downregulated in the mutant, such as the genes encoding cytochrome c oxidase orphan subunits. The early expression of alternative oxidases in the wild type compared with the mutant constitutes a further proof that cyanogenesis occurs earlier than classically assumed and is not solely conditioned by the lack of nutrients or of oxygen occurring at the early stationary phase, where production has been previously reported as being maximal[4]. As expected, differences between the transcriptomes of the wild type and mutant increased over time (Figure 2b,c), with 206 genes (ca. 3.2 % of the genome) dysregulated at the transition between exponential and stationary phase, and 350 (ca. 5.5 %) at late stationary phase, where all COG categories were affected by the presence vs. absence of HCN. These genome-wide expression changes already started at the second time point (transition to stationary phase), where both strains still followed the same growth dynamic (Figure 2a). Overall, the absence of HCN mainly led to gene upregulation, as for instance the genes involved in pyoverdine and phenazine synthesis, which corroborated our phenotypic assays (Figure 2b and Table S2). Similarly, among the few genes upregulated by HCN, we found a helix-turn-helix-type transcriptional regulator (predicted gene name – MlrA) which was strongly downregulated in the HCN-deficient mutant. In *E. coli* and *S. enterica*, MlrA was shown to activate extracellular matrix production[20] and could explain the observed higher biofilm forming capacity of the wild types compared to the HCN-deficient mutants. Higher biofilm formation by wild types could also be explained by higher expression of the type VI secretion system (T6SS) (Figure 1e, Table S2). This system has been shown to be involved in biofilm formation by *P. aeruginosa*[21,22]. Next to its putative role in biofilm formation, the T6SS has been involved in bacterial interactions with competitors, similarly to HCN itself. Likewise, the operon encoding the insecticidal Fit toxin was also among the upregulated ones in the absence of HCN (Table S2), suggesting a possible compensation of the lack of one biological weapon with the higher production of others (e.g., phenazines, pyoverdine, Fit toxin and T6SS). Regarding motility,

transcriptomic analysis revealed upregulation of flagellar biosynthesis genes in the HCN-deficient mutant (Table S2), which could explain both the mutant's higher motility and lower biofilm formation (Figure 1d,e). Altogether, the global transcriptome shifts caused by the presence vs. absence of HCN corroborate the phenotypic differences observed between the wild type and the HCN-deficient mutants (Figure 1) and highlight endogenous HCN as a global regulator of gene expression, compared e.g. with the global activator of secondary metabolism (GacA), whose mutation led to ca 13 % of dysregulated genes in the closely related strain *P. chlororaphis* 30-84[23]. However, the extent of the observed HCN-induced transcriptome changes is in stark contrast to earlier work on *P. aeruginosa*, which reported only 16 dysregulated genes in an HCN-deficient mutant[24]. This discrepancy might be due to a higher resolution of RNA-Seq over microarray analysis, or to different culture conditions, with the complex King's B medium in our case and glycine-enriched minimal medium in the earlier study.

Since HCN is a gaseous molecule easily diffusing into the vicinity of cyanogenic strains, we wondered whether neighbouring, non-cyanogenic cells would respond to exogenous HCN supply with similar changes as those we observed between mutants and wild types. We therefore carried out an experiment where the HCN-deficient mutant of R47 was grown in volatile-mediated contact with its wild type (Figure 3a, Figure S3), and compared both phenotypes and transcriptomes of the wild type, the mutant and the HCN-exposed mutant. Exposing the mutants of both R47 and R32 to exogenous HCN emitted by their respective wild types did not impair the mutants' growth, yet it suppressed the increase in pyoverdine production observed in the non-exposed mutants (Figure 3b) and restored both mutants' biofilm formation to the wild type levels (Figure 3c). For the motility rescue experiment, we observed inconsistent motility in R47 even in the unexposed treatment, possibly due to the split plate experimental setup we used. In R32, we observed swarming rather than swimming motility in

this setup, but for this strain, the phenotype of the HCN-deficient mutant was convincingly rescued upon exposure to HCN (Figure 3d). At the early exponential phase, both non-exposed and exposed mutants of R47 showed similar transcriptome (only 4 differentially expressed genes, see Figure S4 and Table S1), suggesting that at this early time point, HCN was affecting only the producing cells but not yet diffusing into the surrounding plate wells. However, at the later time point corresponding to the transition between exponential and stationary phase, most of the gene expression changes observed in the mutant were rescued by exposure to exogenous HCN (Figure 3e, Figure S4b and c). These included the changes in genes encoding pyoverdine and phenazine synthesis, as well as the MlrA activator, the T6SS and the flagellar biosynthetic genes potentially involved in biofilm formation, which corroborated the rescued phenotypes (Figure 3b,c,d and Table S2). They also included the genes encoding the synthesis of the insecticidal Fit toxin (Figure 3d and Table S2). The transcriptome changes observed at this intermediate time point between the mutant and the exposed mutant mimicked those observed between the mutant and the wild type, confirming that the exposed mutant behaved largely like a wild type (Figure 3b,e). Principal component analysis showed that this transcriptome similarity was further increased at the late stationary phase (time point 3), although the number of dysregulated genes increased from 19 to 141, which might be due to the differential growth between wild type and exposed mutant observed at this later time point (Figure 3b, Figure S4a). Interestingly, the proportion of genes rescued by external supply of HCN at the transition between exponential and stationary phase differed between the COG categories, with a lower rescue proportion in the categories involved in housekeeping functions and primary metabolism (e.g., ribosome structure, replication, energy production, or carbohydrate, amino acid and nucleotide metabolism) than in those potentially involved in biotic interactions (e.g., defence mechanisms, inorganic ion transport and secondary metabolism).

Altogether, our data indicate that HCN's biological functions are much wider than previously thought. Not unlike phenazines, which were also first categorized as "mere secondary metabolites" and which later turned out to act as internal signalling molecules with diverse and important cellular functions[25], we show here that HCN is much more than a respiratory toxin, and acts as an inter- and extracellular signal on both producing and receiving cells. These findings are in line with recent reports on HCN's ability to induce broad physiological effects in both plant and human cells[26,27]. Compared with phenazines, HCN is a volatile molecule and as such, its zone of influence is expected to be much broader[1]. Our data show that this small volatile signalling compound is able to reprogram bacterial behaviour without direct contact, repressing iron uptake, swimming motility and synthesis of biological weapons such as phenazines, the insecticidal Fit toxin or the type VI secretion system. These functional traits are of particular interest in the competitive environments inhabited by cyanogenic *Pseudomonas*, from the plant rhizosphere to the human lung, which further highlight the importance of HCN not only as an intrinsic virulence factor but also, and perhaps more importantly, as a volatile messenger able to manipulate the behaviour of neighbouring cells to the competitive advantage of its producer.

Figures

Figure 1

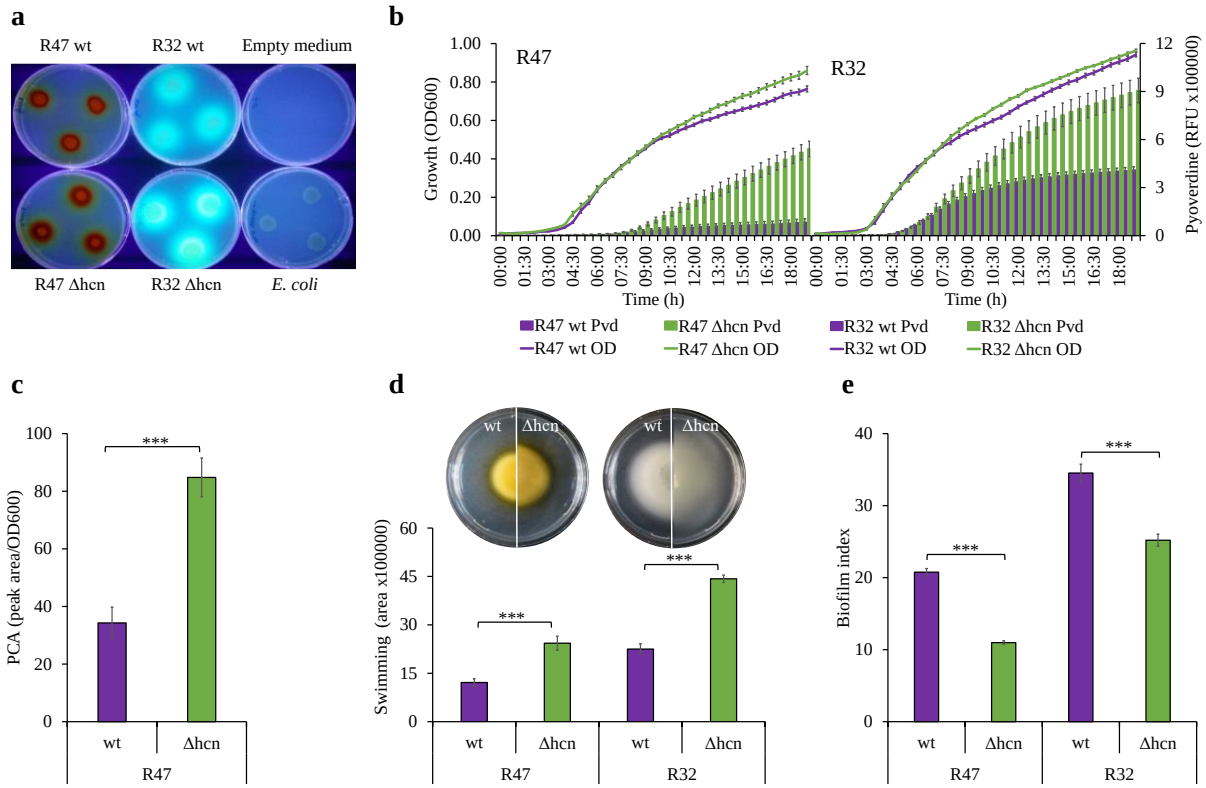

Figure 2

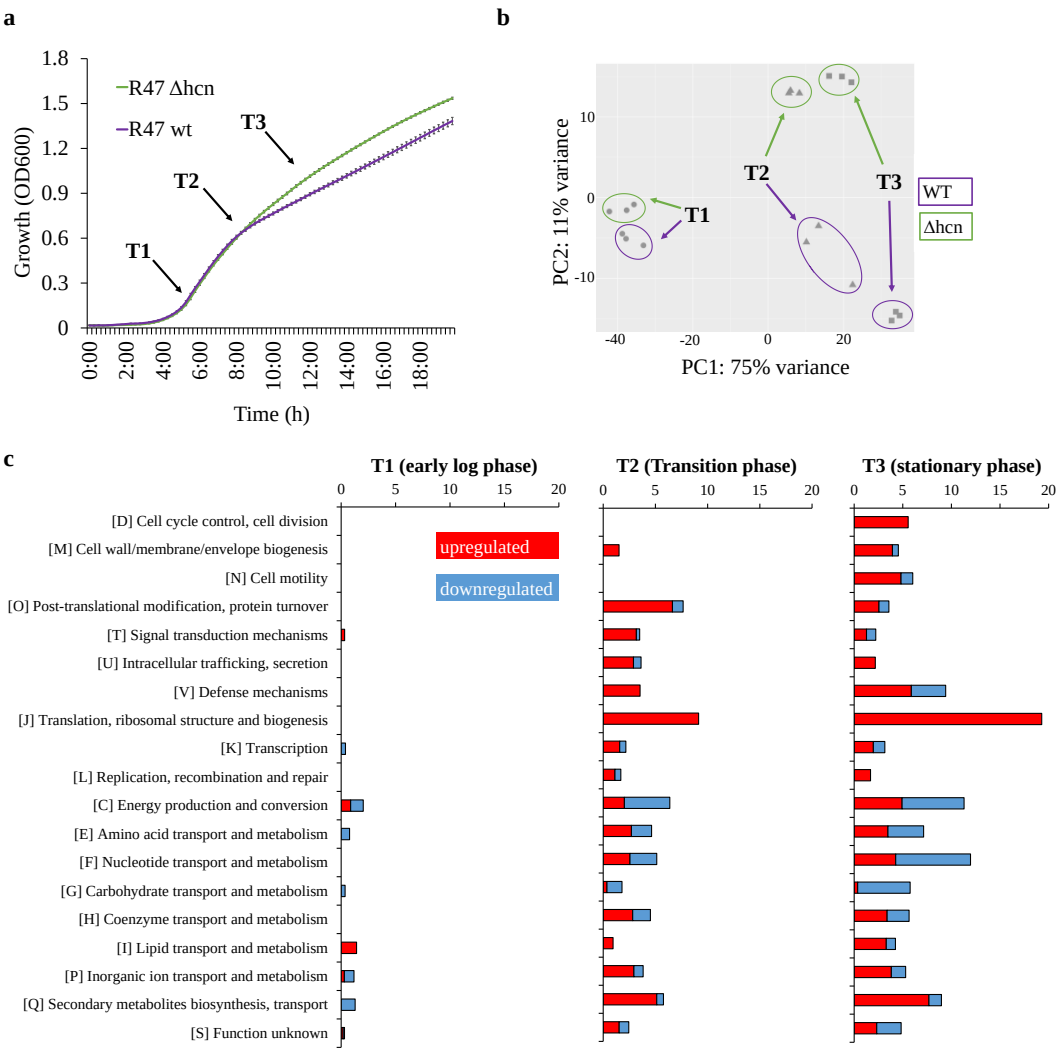
a
R47 Δhcn
R47 wt
T1
T2
T3
Growth (OD600)
Time (h)
b
PC2: 11% variance
PC1: 75% variance
T1
T2
T3
WT
Δhcn
c
T1 (early log phase)
T2 (Transition phase)
T3 (stationary phase)
upregulated
downregulated
[D] Cell cycle control, cell division
[M] Cell wall/membrane/envelope biogenesis
[N] Cell motility
[O] Post-translational modification, protein turnover
[T] Signal transduction mechanisms
[U] Intracellular trafficking, secretion
[V] Defense mechanisms
[J] Translation, ribosomal structure and biogenesis
[K] Transcription
[L] Replication, recombination and repair
[C] Energy production and conversion
[E] Amino acid transport and metabolism
[F] Nucleotide transport and metabolism
[G] Carbohydrate transport and metabolism
[H] Coenzyme transport and metabolism
[I] Lipid transport and metabolism
[P] Inorganic ion transport and metabolism
[Q] Secondary metabolites biosynthesis, transport
[S] Function unknown

Figure 3

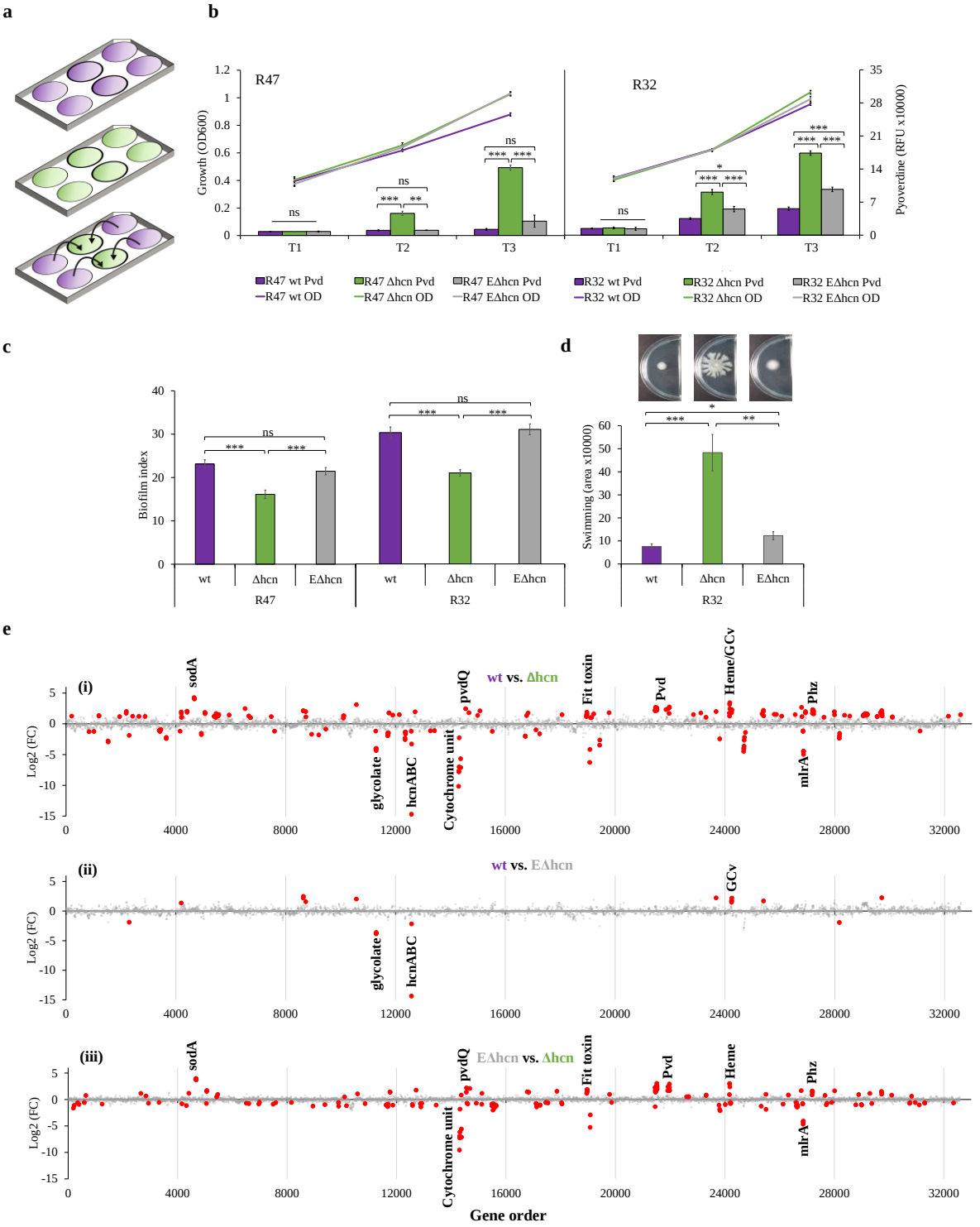
a
b
R47
R32
Growth (OD600)
Pyoverdine (RFU x10000)
T1
T2
T3
ns
***
**
*
R47 wt Pvd
R47 Δhcn Pvd
R47 EΔhcn Pvd
R32 wt Pvd
R32 Δhcn Pvd
R32 EΔhcn Pvd
R47 wt OD
R47 Δhcn OD
R47 EΔhcn OD
R32 wt OD
R32 Δhcn OD
R32 EΔhcn OD
c
Biofilm index
wt
Δhcn
EΔhcn
d
Swimming (area x10000)
e
(i)
wt vs. Δhcn
sodA
glycolate
hcnABC
pvdQ
Cytochrome unit
Fit toxin
Pvd
Heme/GCv
Phz
mlrA
(ii)
wt vs. EΔhcn
GCv
(iii)
EΔhcn vs. Δhcn
Heme
Log2 (FC)
Gene order

Figure legends

Figure 1 | Loss of HCN increases pyoverdine and phenazine production, induces swimming motility and represses biofilm production. a, Qualitative analysis of siderophore production by wild type (wt) and cyanide-deficient (Δhcn) mutant strains of both *P. chlororaphis* R47 and *P. putida* R32 after five days of growth at room temperature on King's B agar medium. Plates were visualised under UV light. b, Growth curve (optical density (OD) at 600nm, lines) and pyoverdine (Pvd) detection assay (fluorescence reading at 465nm, bars) in liquid King's B medium grown for 19h at 30 ˚C. Data represent average of three independent biological replicates with four technical replicates each. c, Phenazine quantification assay based on HPLC-UV detection. Liquid cultures of R47 wt and R47 Δhcn strains were grown at 30 ˚C in liquid King's B medium for 24h before sampling. Bars represent the phenazine carboxylic acid (PCA) peak area normalised with growth (OD600). Data represent average of three independent experiments with three technical replicates in each experiment. d, Swimming motility assay on low agar plates after four to five days incubation at room temperature. Bars represent the colony area covered by the strains on 90 mm plates and measured using the ImageJ software. Bars show average of four and two independent experiments for R47 and R32 respectively, with four to six technical replicates in each experiment. e, Biofilm formation assay. Strains were grown statically in liquid King's B medium in 96-well plates for 48h at 30 ˚C. Bars correspond to biofilm index (crystal violet staining measured at 570 nm divided by optical density measured at 550nm before the staining) and represent the average of three independent experiments with 36 technical replicates each. For c-e, samples were statistically analysed using two-tailed t-test. ***P<0.001. Error bars represent standard error.

Figure 2 | Inability to produce HCN leads to global transcriptional dysregulation. a, Representative growth curve of *P. chlororaphis* R47 wt and Δhcn strains in King's B liquid medium highlighting the three time points used for transcriptomics. T1; early log phase, T2; Transitional phase (exponential to stationary), T3; stationary phase. b, Principal component analysis of transcriptomic data at time points 1, 2, & 3. Strains were grown in King's B liquid medium in 6-well plates at 30 ˚C with continuous shaking before each sampling. c, COG categorical analysis of the dysregulated genes in R47 Δhcn strain compared with its wild type. Bars show percentage of dysregulated genes in each respective COG category. y-axis represents different COG categories. For b & c, data represents RNA-sequencing results that were obtained in three independent experiments. Cut-off for significance; Log2 (fold change) ≥ 1, q-value ≤ 0.05.

Figure 3 | Exposure to exogenous HCN emitted by *P. chlororaphis* wild type represses pyoverdine production, swimming motility but induces biofilm formation in the HCN-deficient mutant. a, Scheme of the volatile-mediated exposure experiment using 6-well plates used for (b). Purple color represents liquid cultures of the wild type, green color liquid cultures of the HCN-deficient mutants. The middle two wells (thicker border) were collected for RNA extraction and sequencing. b, Growth and pyoverdine measurements for *P. chlororaphis* R47 and *P. putida* R32 strains grown at 30 ˚C in liquid King's B medium in 6-well plates. wt, wildtype; Δhcn, cyanide-deficient mutant; EΔhcn, Δhcn strains exposed to HCN emitted by the respective wild types. Measurements were performed as indicated in Figure 1. Data represent

average of three independent experiments with two-six technical replicates each. T1 (early log phase), T2 (transitional phase between exponential and stationary phases) and T3 (stationary phase). c Biofilm formation assay for wild types (wt), HCN-deficient mutants (Δhcn) and HCN-exposed mutants (EΔhcn). The assay was carried out in liquid LB as indicated in Figure 1 and S4. Bars represent average of three independent experiments with 6-20 technical replicates each. d, Swimming motility assay on split Petri dishes. R32 wild type and HCN-deficient mutant were grown on each side of the split Petri dishes. Plates were incubated at room temperature for two days before pictures were taken. The areas were measured as indicated in Figure 1. Bars show averages of two independent experiments with four to five technical replicates each d, Genome wide representation of differentially expressed genes at timepoint 2 (transional phase between exponential and stationary phase) using *P. chlororaphis* R47 genome as reference. The x-axis shows the gene location on the chromosome with each dot corresponding to one gene and the y-axis shows the log2 (fold change) values. (i) and (ii) log2 (fold change) values correspond to Δhcn and EΔhcn using wt as reference repectively. (iii) Log2 (fold change) values correspond to Δhcn strain using EΔhcn as reference. Red dots represent significantly differentially expressed genes while grey dots represent no significant difference as compared to the respective reference. Cut-off for significane; Log2 (fold change) ≥ 1, q-value ≤ 0.05. For b-d, samples were statistically analysed using two-tailed *t*-test. Error bars represent the standard error. ***$P<0.001$, **$P<0.01$, *$P<0.05$; ns, not significant. For e, dots represent average values from three independent experiments for each time point and treatment. sodA, superoxide dismutase A; hcnABC, hydrogen cyanide synthase ABC; cytochrome unit, cytochrome orhan subunit N4Q4; Pvd, pyoverdine biosynthesis genes; Phz, phenazine biosynthesis genes; glycolate, glycolate to glyoxylate oxidation; heme, heme utilisation genes; mlrA, activator of csgD (master regulator of biofilm formation); Fit toxin, Fit toxin biosynthesis genes.

Experimental procedures

Strains and culture media

Pseudomonas chlororaphis (R47) and *Pseudomonas putida* (R32) and their derived Δhcn mutants were grown/maintained at 30 ˚C on Lysogeny broth (LB) agar medium (20 g/L of LB mix (Lennox, Fisher Bioreagents) with 15 g/L of agar (Agar-agar, Kobe I, Carl Roth))[28]. Generation of Δhcn strains has been previously described[13]. King's B (KB) medium was prepared by mixing 20 g/L of proteose peptone #3 (Bacto™ Proteose Peptone No. 3, ThermoFisher Scientific), 1.5 g/L of dipotassium phosphate (Carl Roth GmbH + Co. KG), 1.5 g/L of magnesium sulfate heptahydrate (Carl Roth GmbH + Co. KG) and 10ml/L of glycerol (Carl Roth GmbH + Co. KG) and 15 g/L of agar (when needed).

Growth curves and pyoverdine measurements

Bacterial colonies (two-three single colonies) were used to inoculate LB broth and cultured for 19h at 30 ˚C with shaking (180 rpm). The cells were collected by centrifugation at 5000 rpm for five min and then washed twice with 0.9 % NaCl. The bacterial suspension was then adjusted to OD600 = 1 (henceforth named 'OD adjusted') and 5 µl was used to inoculate 100 µl of KB broth in 96-well plates (Corning, NY, USA). Parafilm was used to seal the plates. Cytation5 automated plate reader (BioTek, Winooski, VT, USA) was used to incubate plates at 30 ˚C with continuous shaking. Reads were taken at 600 nm to generate growth curves and pyoverdine measurements were done at excitation = 405 nm and emission = 460 nm[15]. For HCN exposure experiments, similar readings were taken with 6-well plates (Corning, NY, USA) (Figure 3a). Three ml KB broth was added to each well and 300 µl of OD adjusted bacteria were added. Plates were incubated at 30 ˚C with shaking at 90 rpm and readings were taken for 5, 7 & 11h. All experiments were replicated thrice independently in total.

Phenazine measurement and identification

Phenazines were quantified as previously described using a high-performance liquid chromatography (HPLC) method[29]. Briefly, OD adjusted bacterial cells were inoculated in 5ml King's B broth and incubated at 30 °C with shaking at 180 rpm for 24 h. The culture was then filtered using 0.2 µm filter (Fisher Scientific International, Inc.) and stored at -20°C until analysis. Analyses were performed by a HPLC equipped with a quaternary pump P100A, coupled with a UV diode array detector ultimate 3000 (Dionex, Thermoscientific, Olten, Switzerland). The samples (40µl) were injected onto a MN Nucleosil C18 analytical column (250 mm x 4 mm i.d., 100-5) (Macherey-Nagel, Duren, Germany), using a flow rate of 0.8 $mL.min^{-1}$ at 27°C. The mobile phase consisted of solvent A (0,1% TFA (trifluoroacetic acid) in water) and solvent B (0,1% TFA in acetonitrile) ; the gradient started with 5 % of solvent B and reached 15 % at 2 min, 83% at 15 min, 95% at 16 min, and 100% at 45 min. Phenazines were detected at 365 and 250 nm with diode array on-line detection. UV spectra were recorded between 200 and 800 nm. For compound identification, samples were freeze dried, dissolved in 500 µl of ethyl acetate and purified by preparative TLC on silica gel (Kieselgel 60, F_{254}, 0.25, Merck, Darmstadt, Germany) using CHCl3: MeOH (95:5) as the eluent. The spots were visualized by exposure to UV radiation at 256 nm. Three compounds were isolates and identified by HPLC and mass spectrometry as 1 or 2- hydroxyphenazine (i) (Rf 0.72; Rt 14.55; m/z 197.07 $[M+H]^+$), phenazine-1-carboxylic acid (PCA) (ii) (Rf 0.64; RT 1.,4; m/z 225.06 $[M+H]^+$) and 2-hydroxyphenazine carboxylic acid (iii) (Rf 0.58; Rt.21.23; m/z 241.06 $[M+H]^+$). ESI-MS/MS analysis in positive ionisation mode were performed on Q Exactive Plus (Thermo Fisher Scientific). Mass spectra were recorded between 50 and 500 *m/z*. The peak areas at the

specific wavelength λ_{max} 250 nm were chosen for qualitative quantification. Three biologically independent replicates were collected with three technical replicates in each experiment.

Swimming motility assay

Swimming motility assay was performed as previously reported[30]. Briefly, OD adjusted inoculum was pricked into the 0.3% M9 agar medium (For 1 litre, 10 ml of 20 % glucose (Carl Roth GmbH + Co. KG), 10 ml of 20 % casamino acids (Bacto™, Difco Laboratory), 1 ml of 1M $MgSO_4$ (Carl Roth GmbH + Co. KG), 3 g agar (Agar-agar, Kobe I, Carl Roth), 200 ml of 5X M8 solution (64 g $Na_2HPO_4.7H_2O$ (Carl Roth GmbH + Co. KG), 15 g KH_2PO_4 (Carl Roth GmbH + Co. KG), 2.5g NaCl (Acros Organics) for 1 litre)) in 90-mm Petri plates which were incubated in upright position for four to five days at room temperature. The experiment was replicated independently four times for R47 and twice for R32. For exposure experiments, split Petri dishes were used. LB agar was poured on one side of the dish and 0.3% M9 minimal agar medium was poured on the other side. Ten ml of medium were poured on each side of the Petri dish. LB agar side was inoculated with three 10 µl drops of OD adjusted bacterial suspension while the M9 agar side was pricked at the centre with a pipette tip. The LB side of the plate was inoculated 6h before inoculation on the M9 agar side. Plates were incubated at room temperature for two days. The pictures were taken and analysed using the ImageJ software[31] to obtain the growth area in pixels square. The experiment was replicated independently twice. Plates were parafilmed before incubation.

Biofilm formation assays

Bacterial collection and inoculation in liquid King's B medium was as described in '*Growth curves and pyoverdine measurements*'. The inoculated plates (96-well plates, Corning, NY, USA) were statically incubated at 30 ˚C for 48h and biofilm measurements were done as previously reported[32] using a Cytation5 plate reader (BioTek, Winooski, VT, USA). The experiment was replicated thrice in total with 36 technical replicates each. For exposure experiments, 24-well plates (Corning, NY, USA) were used. 100 µl of OD adjusted bacterial cells were added to 1 ml of LB broth and plates were incubated for 48h statically at 30 ˚C. A schematic of the experimental setup is shown in Figure S5. Exposure experiments were independently reproduced three times with 6-20 technical replicates. Parafilm was used to seal the plates for all biofilm experiments.

RNA extraction

OD adjusted bacterial cells were inoculated in 6-well plates (Corning, NY, USA) at a final OD600 = 0.1 in KB broth. The plates were then sealed with parafilm. The experimental setup is shown in Figure 3a. For all three time points, cells equivalent to OD600 = 3 were collected from the middle two wells (dark boundary in figure 3a) by centrifugation at 5000 rpm for 5min at 4 ˚C. Samples from each treatment and time point were collected in three independent experiments. The collected cells were flash frozen using liquid nitrogen and stored at -80 ˚C until RNA extraction. RNA extraction was performed using standard phenol-chloroform extraction using the Trizol method[33]. Samples were treated with DNaseI (Sigma Aldrich) and then re-extracted using the same Trizol method as above. The RNA was quantified and analysed by the NGS facility in Bern (using both Qubit and Bioanalyser quantification). The libraries were prepared according to the TruSeq Stranded mRNA Sample Preparation Guide (Illumina). Briefly, total RNA was purified, fragmented, reverse transcribed, and amplified to generate the libraries, which were subjected to high-throughput 100bp single-end sequencing on a NovaSeq 6000 instrument (Illumina).

RNA-seq data analysis, Statistical analysis

Quality control of the reads was performed with FastQC v0.11.7 (fastqc: https://www.bioinformatics.babraham.ac.uk/projects/fastqc/), revealing excellent quality reads for all samples. The reads were cleaned using fastp v0.19.5[34] with a special focus on removing polyG trails and keeping only full length reads (100bp). The reference genome for *Pseudomonas chlororaphis* R47 (CP019399) was downloaded from the NCBI and indexed for STAR v2.5.0b[35]. Then the reads of each sample from step 1 were remapped to genes with STAR using the annotation information (gtf file). The final table of counts was obtained by merging the individual tables with unix commands. The read counts were then analysed using the R library DESeq2, version 1.30.1[36]. Log2 (fold change) cut-off was set to greater than equal to 1 and adjusted p-value threshold was set to greater than equal to 0.05.

qPCR analysis

Three biologically independent samples collected for RNA-seq were analysed for the expression of hcnA gene. Primers used are described in table S3. RNA samples were reverse transcribed using SensiFAST cDNA synthesis kit (Bioline). Quantitative PCR was performed according to the manufacturer's instructions (Bioline). Briefly, 25 ng of cDNA was mixed with 0.5 µl of forward and reverse primers, 1.5 µl of sterile water and 7.5 µl SYBR Hi-ROX mix (Bioline). Reaction conditions were as follows; 95 ˚C for 15min (initial denaturation), 45 cycles of 95 ˚C for 15s, 60 ˚C for 15s, 72 ˚C for 30s. Data was analysed using the delta Cq method.

References

1. Weisskopf, L., Schulz, S. & Garbeva, P. Microbial volatile organic compounds in intra-kingdom and inter-kingdom interactions. *Nature Reviews Microbiology* (2021) doi:10.1038/s41579-020-00508-1.
2. Voisard, C., Keel, C., Haas, D. & Defago, G. Cyanide production by Pseudomonas fluorescens helps suppress black root rot of tobacco under gnotobiotic conditions. *EMBO J.* **8**, 351–358 (1989).
3. Wilson, M. T., Antonini, G., Malatesta, F., Sarti, P. & Brunori, M. Probing the oxygen binding site of cytochrome c oxidase by cyanide. *J. Biol. Chem.* **269**, 24114–24119 (1994).
4. Blumer, C. & Haas, D. Mechanism, regulation, and ecological role of bacterial cyanide biosynthesis. *Arch. Microbiol.* **173**, 170–177 (2000).
5. Ryall, B., Davies, J. C., Wilson, R., Shoemark, A. & Williams, H. D. Pseudomonas aeruginosa, cyanide accumulation and lung function in CF and non-CF bronchiectasis patients. *Eur. Respir. J.* **32**, 740–747 (2008).
6. Haas, D. & Défago, G. Biological control of soil-borne pathogens by fluorescent pseudomonads. *Nat. Rev. Microbiol.* **3**, 307–319 (2005).
7. Gunasekar, P. G., Borowitz, J. L., Turek, J. J., Van Horn, D. A. & Isom, G. E. Endogenous generation of cyanide in neuronal tissue: Involvement of a peroxidase system. *J. Neurosci. Res.* **61**, 570–575 (2000).
8. Bröckner, A. *et al.* Storage and release of hydrogen cyanide in a chelicerate (Oribatula tibialis). *Proc. Natl. Acad. Sci. U. S. A.* (2017) doi:10.1073/pnas.1618327114.
9. Peiser, G. D. *et al.* Formation of cyanide from carbon 1 of 1-aminocyclopropane-1-carboxylic acid during its conversion to ethylene. *Proc. Natl. Acad. Sci.* **81**, 3059–3063 (1984).
10. Williams, H. D., Zlosnik, J. E. A. & Ryall, B. *Oxygen, Cyanide and Energy Generation in the Cystic Fibrosis Pathogen Pseudomonas aeruginosa*. *Advances in Microbial Physiology* vol. 52 (2006).
11. Zdor, R. E. Bacterial cyanogenesis: Impact on biotic interactions. *J. Appl. Microbiol.* **118**, 267–274 (2015).
12. De Vrieze, M. *et al.* Linking comparative genomics of nine potato-associated Pseudomonas isolates with their differing biocontrol potential against late blight. *Front. Microbiol.* **11**, 857 (2020).
13. Anand, A. *et al.* Contribution of hydrogen cyanide to the antagonistic activity of pseudomonas strains against phytophthora infestans. *Microorganisms* (2020) doi:10.3390/microorganisms8081144.
14. Kloepper, J. W., Leongt, J., Teintzet, M. & Schroth, M. N. Enhanced plant growth by siderophores produced by plant growth-promoting rhizobacteria. *Nature* **286**, 885–886 (1980).

15. Kang, D. & Kirienko, N. V. High-throughput genetic screen reveals that early attachment and biofilm formation are necessary for full pyoverdine production by Pseudomonas aeruginosa. *Front. Microbiol.* (2017) doi:10.3389/fmicb.2017.01707.

16. Mavrodi, D. V., Blankenfeldt, W. & Thomashow, L. S. Phenazine Compounds in Fluorescent Pseudomonas Spp. Biosynthesis and Regulation. *Annu. Rev. Phytopathol.* **44**, 417–445 (2006).

17. O'Toole, G., Kaplan, H. B. & Kolter, R. Biofilm formation as microbial development. *Annual Review of Microbiology* (2000) doi:10.1146/annurev.micro.54.1.49.

18. Morris, C. E. & Monier, J. M. The Ecological Significance of Biofilm Formation by Plant-Associated Bacteria. *Annual Review of Phytopathology* (2003) doi:10.1146/annurev.phyto.41.022103.134521.

19. Castric, P. A. Hydrogen cyanide, a secondary metabolite of Pseudomonas aeruginosa. *Can. J. Microbiol.* **21**, 613–618 (1975).

20. Brown, P. K. *et al.* MIrA, a novel regulator of curli (AgF) and extracellular matrix synthesis by Escherichia coli and Salmonella enterica serovar typhimurium. *Mol. Microbiol.* **41**, 349–363 (2001).

21. Southey-Pillig, C. J., Davies, D. G. & Sauer, K. Characterization of temporal protein production in Pseudomonas aeruginosa biofilms. *J. Bacteriol.* (2005) doi:10.1128/JB.187.23.8114-8126.2005.

22. Gallique, M., Bouteiller, M. & Merieau, A. The type VI secretion system: A dynamic system for bacterial communication? *Front. Microbiol.* **8**, 1–10 (2017).

23. Wang, D. *et al.* Roles of the Gac-Rsm pathway in the regulation of phenazine biosynthesis in Pseudomonas chlororaphis 30-84. *Microbiologyopen* **2**, 505–524 (2013).

24. Frangipani, E., Pérez-Martínez, I., Williams, H. D., Cherbuin, G. & Haas, D. A novel cyanide-inducible gene cluster helps protect Pseudomonas aeruginosa from cyanide. *Environ. Microbiol. Rep.* **6**, 28–34 (2014).

25. Price-Whelan, A., Dietrich, L. E. P. & Newman, D. K. Rethinking 'secondary' metabolism: Physiological roles for phenazine antibiotics. *Nat. Chem. Biol.* **2**, 71–78 (2006).

26. Randi, E. B., Zuhra, K., Pecze, L., Panagaki, T. & Szabo, C. Physiological concentrations of cyanide stimulate mitochondrial Complex IV and enhance cellular bioenergetics. *Proc. Natl. Acad. Sci. U. S. A.* **118**, (2021).

27. García, I., Arenas-Alfonseca, L., Moreno, I., Gotor, C. & Romero, L. C. HCN regulates cellular processes through posttranslational modification of proteins by s-cyanylation. *Plant Physiol.* **179**, 107–123 (2019).

28. Hunziker, L. *et al.* Pseudomonas strains naturally associated with potato plants produce volatiles with high potential for inhibition of Phytophthora infestans. *Appl. Environ. Microbiol.* **81**, 821–830 (2015).

29. Kern, S. E. & Newman, D. K. Measurement of phenazines in bacterial cultures. *Methods Mol. Biol.* (2014) doi:10.1007/978-1-4939-0473-0_25.

30. Ha, D. G., Kuchma, S. L. & O'Toole, G. A. Plate-Based assay for swimming motility in pseudomonas aeruginosa. *Methods Mol. Biol.* (2014) doi:10.1007/978-1-4939-0473-0_7.

31. Schneider, C. A., Rasband, W. S. & Eliceiri, K. W. NIH Image to ImageJ: 25 years of image analysis. *Nature Methods* (2012) doi:10.1038/nmeth.2089.

32. Coffey, B. M. & Anderson, G. G. Biofilm formation in the 96-well microtiter plate. *Methods Mol. Biol.* (2014) doi:10.1007/978-1-4939-0473-0_48.

33. Chomczynski, P. & Sacchi, N. Single-step method of RNA isolation by acid guanidinium thiocyanate-phenol-chloroform extraction. *Anal. Biochem.* (1987) doi:10.1016/0003-2697(87)90021-2.

34. Chen, S., Zhou, Y., Chen, Y. & Gu, J. Fastp: An ultra-fast all-in-one FASTQ preprocessor. in *Bioinformatics* (2018). doi:10.1093/bioinformatics/bty560.

35. Dobin, A. *et al.* STAR: Ultrafast universal RNA-seq aligner. *Bioinformatics* (2013) doi:10.1093/bioinformatics/bts635.

36. Love, M. I., Huber, W. & Anders, S. Moderated estimation of fold change and dispersion for RNA-seq data with DESeq2. *Genome Biol.* (2014) doi:10.1186/s13059-014-0550-8.

Acknowledgements

Financial support from the Swiss National Science Foundation (grant 179310 to LW) is gratefully acknowledged.

Author Contributions

LW and AA conceived the project and wrote the manuscript, with help from CK. AA performed all experiments, with help from FLH. LF performed transcriptomics analysis, EAM performed HPLC analysis. All authors commented on the manuscript.

Competing Interests statement

The authors declare no competing interests.